# Tunneling Current and Electroluminescence in InGaN: Zn,Si/AlGaN/GaN Blue Light Emitting Diodes

PETR G. ELISEEV,* PIOTR PERLIN,† JULIEN FURIOLI,‡ PHILIPPE SARTORI,‡ JIAN MU, and MAREK OSIŃSKI

Center for High Technology Materials, University of New Mexico, Albuquerque, NM 87131-6081

We investigate electrical and optical characteristics of Nichia NLPB-500 double-heterostructure blue light-emitting diodes (LEDs), measured over a wide temperature range from 10 to 300K. Current-voltage characteristics have complex character and suggest involvement of at least two different tunneling mechanisms. The peak energy of the optical emission follows the applied bias for voltages between 2.3–2.6 V and can be tuned in large spectral range from 2.3 up to 2.8 eV (yellow to blue). This behavior can be understood invoking the photon-assisted tunneling model which was previously successfully applied to highly doped GaAs LEDs. Even at the lowest temperatures, light emission still continues while the increase in the series resistance does not exceed a few tens of kΩ, which indicates absence of complete carrier freeze-out.

**Key words:** Gallium nitride, light-emitting diodes, tunneling

## INTRODUCTION

Group-III nitride wide-bandgap semiconductors are very attractive for fabrication of light emitting (LEDs) and diode lasers emitting in the short-wavelength visible and ultraviolet (UV) part of spectrums.[1–3] Recent rapid progress in commercialization of blue and green InGaN/AlGaN/GaN LEDs has left unresolved many fundamental issues associated with material and device properties. The main goal of this paper is to elucidate some of these issues by carrying out electrical and optical characterization of high-brightness NLPB-500 double-heterostructure blue LEDs manufactured by Nichia Chemical Industries, with the active region codoped with Zn and Si.[2]

Electrical characteristics of LEDs can provide important information about current transport through the wide-bandgap p-n heterojunction, metal-semiconductor contacts, and layer materials. In a recent computer simulation of GaN-based LEDs,[4] thermionic emission over bandgap discontinuity spikes was included, but its effect was rather small, with thermally limited current-voltage (I-V) characteristics. In contrast, previous experimental studies[5–7] had identified tunneling as a dominant transport mechanism over a wide bias range. In Ref. 5, large values of the nonideality factor n of I-V curves were reported for NLPB-500 LEDs (n = 5 at room temperature, and up to n = 50 at T = 80K). The LEDs were shown[6–8] to operate at very low temperatures (down to ~9K) with no sign of conductivity freeze-out.

In this paper, we give a more detailed account of our studies of NLP-B500 LEDs. We discuss how series resistance and p-n junction contributions to I-V characteristics can be separated. Electrical properties of LEDs are then interpreted in terms of tunneling currents. The emission spectra are studied over a wide range of operating conditions, including cryogenic temperatures and high-current-amplitude pulsed operation.

*On leave from P.N. Lebedev Physics Institute, Russian Academy of Sciences, Moscow, Russia
†On leave from High Pressure Research Center, Warsaw, Poland
‡Present address: Ecole Nationale Supérieure des Télécommunications, Paris, France
(Received September 22, 1996; accepted December 7, 1996)

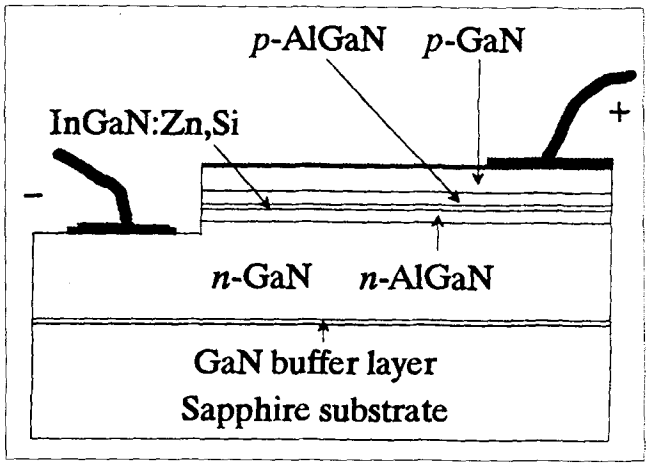


Fig. 1. Schematics of the Nichia DH blue LED with InGaN emitting layer grown on the sapphire substrate (after Ref. 2). Layer thickness are as follows: GaN buffer layer, 30 nm; n-GaN:Si layer, 4 mm; n-$Al_{0.15}Ga_{0.85}N$:Si cladding layer, 150 nm; $In_{0.06}Ga_{0.94}N$:Zn,Si active layer, 50 nm; p-$Al_{0.15}Ga_{0.85}N$:Mg cladding layer, 150 nm; p-GaN:Mg layer, 500 nm. Contacts are Ni/Au on p-side, and Ti/Al on n-side.

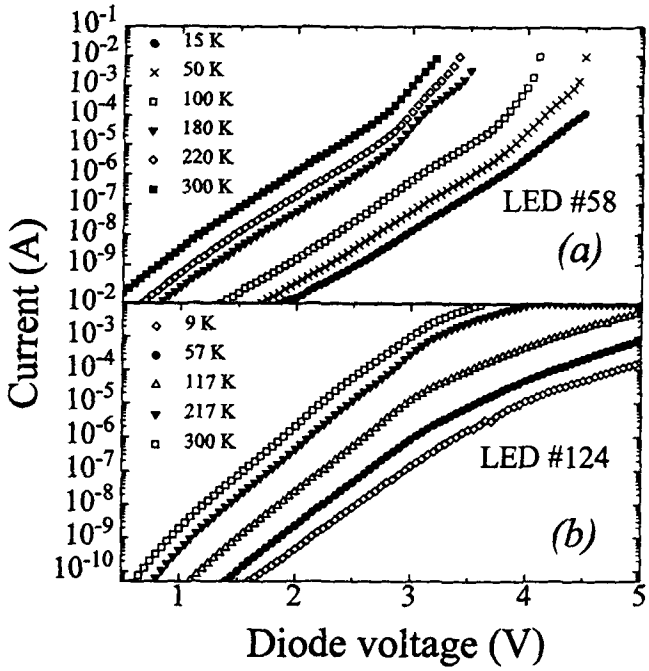


Fig. 2. I-V characteristics at temperatures from 9 to 300K for (a) an old generation LED #58, and (b) a new generation LED #124.

## EXPERIMENT

The samples under investigation were Nichia NLPB-500 double-heterostructure (DH) blue LEDs, illustrated schematically in Fig. 1. The devices were grown on nonconducting sapphire substrates and cut into ~350 μm × 350 μm squares. The total thickness of the chip, including the sapphire substrate, is ~85 μm. In order to expose the n-side for electrical contact, about a quarter of the chip was etched down through the active region. The remaining junction area was ~$9 \times 10^{-4}$ $cm^2$. The blue and blue-green electroluminescence (EL) results from efficient recombination of carriers at Zn-related deep levels[2,9] in the active layer co-doped with Zn and Si, similarly to the emission mechanism in GaN:Zn.[10,11]

The LEDs investigated originated from two production lots: lot #S403024 acquired in March 1994 (called here the "old generation"), and lot #4B0001 acquired in April 1995 (called here the "new generation"). Samples from the earlier lot are labeled here with numbers smaller than 100, while labels of new generation samples are greater than 100. As described in the next section, our measurements revealed significant differences between the devices from these two lots, with an improved external quantum efficiency of new generation LEDs (~3.5% at room temperature, compared to ~2.0–2.5% in the old generation LEDs), different I-V characteristics, and much weaker band-to-band emission in the new generation LEDs.

The I-V characteristics and emission spectra were obtained over a wide temperature range (9–340K). Prior to measurements, an old generation diode #58 and a new generation diode #124 were de-encapsulated to avoid the risk of epoxy-induced stress at cryogenic temperatures. The dc I-V characteristics were measured using a Hewlett-Packard 4140B picoamperometer which can register currents as low as 10 pA. High-current excitation was also performed with 100-ns pulsewidth at the repetition rate of up to 10 kHz. For low temperature measurements, the LED was fixed on a cold finger of either a micro-refrigeration device (MMR Technologies, model K2001) or a closed-cycle refrigerator (CTI-Cryogenics, model 22). Optical experiments were performed using an Acton SpectraPro 27.5 cm monochromator, equipped with a GaAs (R-639) photomultiplier.

## EXPERIMENTAL RESULTS

### I-V Characteristics

Typical I-V curves for LEDs of both generations are shown in Fig. 2. Straight-line segments on a semilogarithimic plot correspond to simple exponential functions. In Fig. 2a (old generation), at least two main exponential segments of different slopes can be easily distinguished; while in Fig. 2b (new generation), only one such segment can be clearly seen. Sublinear behavior at large bias in Fig. 2b suggests that the current in new generation LEDs is limited by a higher series resistance, and details of carrier transport across the p-n junction cannot be readily observed in the high-bias regime. For this reason, we have to identify and subtract the contribution of series resistance $R_s$ of the diode (i.e., the contribution of bulk layers and of metal-semiconductor contacts) in I-V characteristics. In view of a complex structure of the device and nonlinear electrical characteristics, this task turned out to be quite nontrivial.

An estimate of $R_s$ can be made based on the high-current part (>1 mA) of the I-V curves, usually dominated by the series resistance, by plotting the differential resistance of the diode dV/dI vs 1/I and extrapolating to $1/I \rightarrow 0$. For the old generation LEDs,

this gives 5–15 Ω at room and higher temperatures, increasing to 50–100 Ω at 80K, and to the kΩ range at liquid-helium temperature. The new generation samples had a higher series resistance, limiting the current above 3-V bias (cf. Fig. 2b), with $R_s$ exceeding 10 kΩ at T ≈ 10K.

Alternatively, the voltages at the junction $V_j$ and at the series resistance $V_R$ (= $IR_s$) can be separated by assuming that in the low-current range (where the series resistance contribution is negligible) the function I(V) is practically identical with $I(V_j)$. The high-current part of $I(V_j)$ can then be estimated by extrapolation from the low-current part. If the series resistance is not itself current-dependent and our assumption of exponential form of $I(V_j)$ is correct, these two methods should give almost the same result.

For new generation devices, the procedure of finding $R_s$ by assuming a simple exponential extrapolation of the function $I(V_j)$ over the whole voltage range and a current-independent series resistance worked well at liquid-nitrogen and higher temperatures. At lower temperatures, however, the experimental results could not be fitted with a current-independent value of $R_s$. This is illustrated in Fig. 3, indicating that low-temperature $R_s$ in nitride-based LEDs decreases with an increasing current. We shall return to this subject in the discussion section.

Figure 4 shows the series voltage ($V_R$ = $IR_s$) dependence of $R_s$ obtained for the LED #124 at 9K. At low series voltages ($V_R$ = $IR_s$ less than ~50 mV), $R_s$ is close to 100 kΩ and drops down more than an order of magnitude to ~5 kΩ at $V_R$ = 0.8 V. The decrease of $R_s$ seems to obey the $V_R^{-3/2}$ law, as shown by the straight line in Fig 4. Assuming that the main contribution to series voltage arises from relatively highly resistant p-AlGaN layer with 150 nmj thickness, we estimate the electric field strength at which $R_s$ starts to decrease to be close to 7 kV/cm. The effect of reduction of $R_s$ with increasing voltage is strongest at very low temperatures and is constrained to a factor of 1.2–1.5 at 80K.

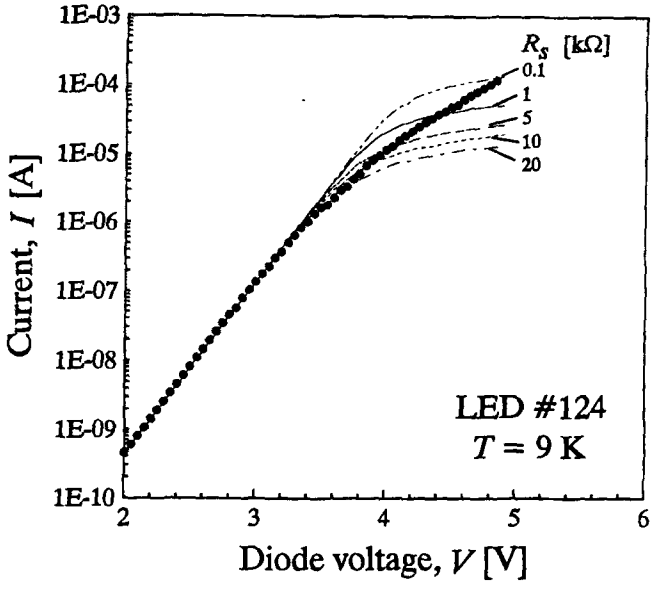


Fig. 3. Low temperature I-V and L-V characteristics of the new-generation LED #124. Several solid curves represent corrections for various constant values of series resistance, obtained by plotting $I(V_j) = I(V - Ir_s)$, with constant $R_s$ between 5 and 40 kΩ, and exponential $I(V_j)$. It is clear that the measured curve (full circles) does not follow any of the calculated curves, but instead crosses them over, indicating a change in $R_s$. The L-V data are shown as measured (open circles) and converted to junction voltage assuming $R_s$ = 20 kΩ (crosses).

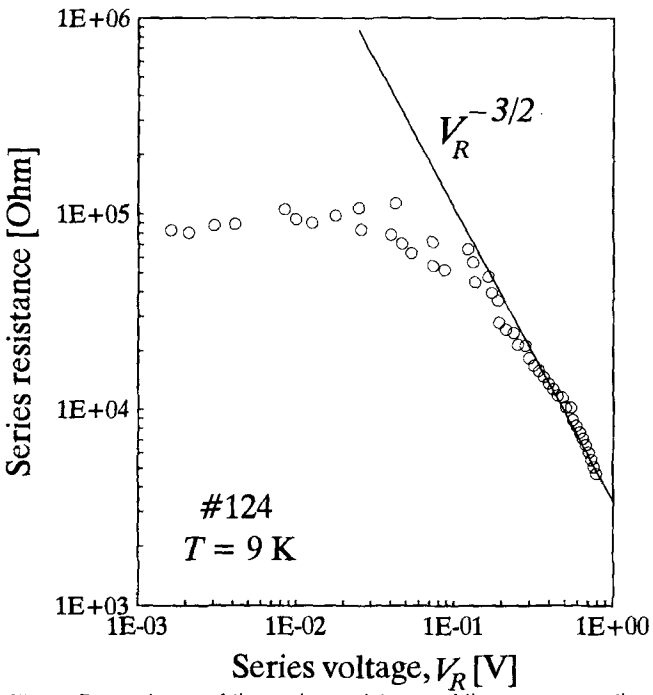


Fig. 4. Dependence of the series resistance of the new-generation LED #124 on the series voltage drop $V_R$ as derived from the I-V curve at 9K. The straight line represents the $V_R^{-3/2}$ dependence.

**Table I. Energy Parameters of I-VCharacteristics for Various Investigated LEDs**

| Temp. Range K | Parameter [meV] | LED #A | LED #48 | LED #58 | LED#124 |
|---|---|---|---|---|---|
| 9–20 | $E_1$ | — | — | 185 | 170 |
| | $E_2$ | — | — | 92 | |
| 77–100 | $E_1$ | 217 | 185 | 185 | 160 |
| | $E_2$ | 87 | 59 | 80 | — |
| 180–200 | $E_1$ | — | 185 | 180 | 150 |
| | $E_2$ | — | 55 | 70 | — |
| 280–300 | $E_1$ | 189 | 182 | 180 | 145 |
| | $E_2$ | 85 | 48 | 70 | — |

Note: Sample #124 differs by a higher Zn concentration in the active region (the second component was not determined in this sample).

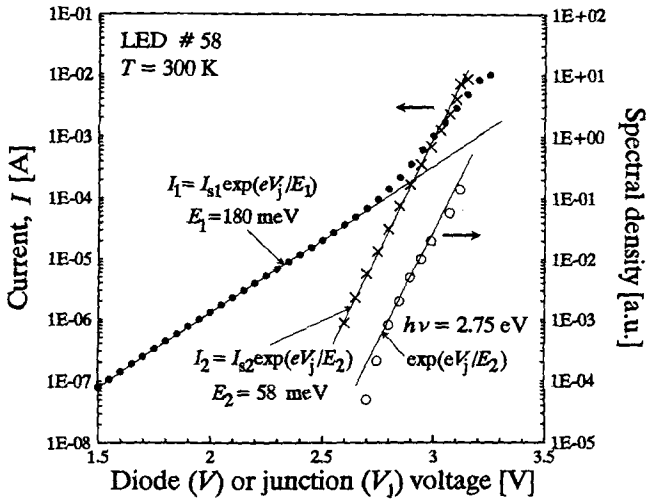


Fig. 5. Analysis of the room-temperature I-V curve (full circles, total current vs the diode voltage) for two nearly exponential components. Data for second component (shown by crosses) are plotted vs junction voltage being corrected for the voltage drop at series resistance of 40 Ω. Open circles are drawn for the blue light intensity in the spectral band peaked at 2.75 eV vs the junction voltage.

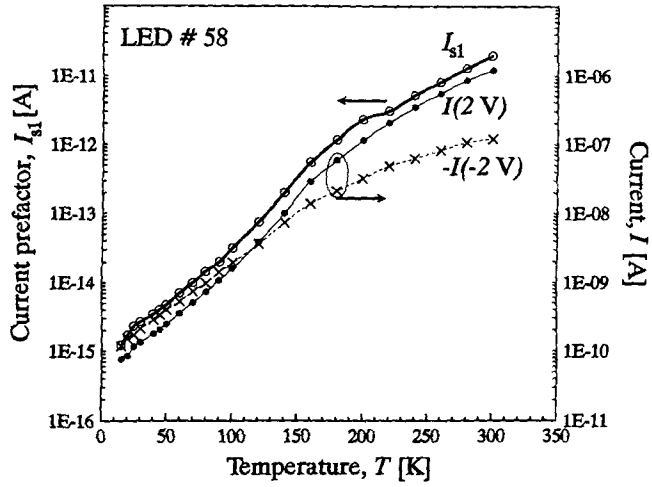


Fig. 6. Temperature dependencies of the pre-exponential factor $I_s$ of the low-voltage current component (open circles), forward current measured at 2 V bias (solid line) and reverse current measured at –2 V bias (crosses) for the old-generation LED #58.

The most striking feature of I-Vcharacteristics, common to both LED generations, is the very weak temperature dependence of the slope of I-V curves on a semilogarithmic plot, in sharp contrast to the standard Shockley model of a diode. For old-generation devices, we can distinguish two different current components: *a low-voltage component* dominant at voltages lower than 2.9 V, and *a medium-voltage component* dominant above 2.9 V. Both components can be well approximated by the exponential functions

$$I_1 = I_{s1}\left[\exp\left(eV_j/E_1\right) - 1\right], \qquad V_j \geq 0 \qquad (1a)$$

$$I_2 = I_{s2}\left[\exp\left(eV_j/E_2\right) - 1\right], \qquad V_j \geq 0 \qquad (1b)$$

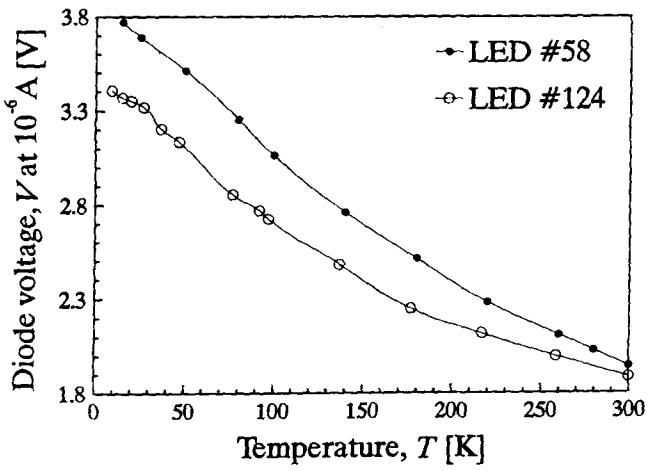


Fig. 7. Temperature dependence of the diode voltage at 1-μA current.

with the electron charge e, pre-exponential factors $I_{s1}$, $I_{s2}$, and energy parameters $E_1$, $E_2$. Values of both $E_1$ and $E_2$ are given in Table I for a number of samples investigated and a range of temperatures. Weak dependence of $E_1$ and $E_2$ on temperature indicates that the dominant transport mechanism is associated with tunneling of carriers rather than thermal diffusion. In the medium voltage range (2.9–3.6 V), the I-V curves are influenced by an increasing voltage drop at the series resistance $R_s$, and by a change in the predominant mechanism of current transport across the junction. The latter is manifested by an increase in the I-V curve slope on the semilogarithmic scale, typically above 10 μA. The medium-voltage component may be singled out after subtracting the extrapolated low-voltage component from the total current. In the case of new generation devices, the medium-voltage component is not apparent in Fig. 2b because it is masked by a large series resistance.

The analysis of the room-temperature I-V curve is given in Fig. 5 for an old-generation LED #58, with inclusion of data for emission intensity vs the junction voltage. Two current components are separated, with $E_1$ = 180 meV and $E_2$ = 58 meV. It can be clearly seen that the blue emission intensity in the 2.75-eV spectral band is evolving in parallel with the medium-voltage current component. On the other hand, the intensity of the 3.2-eV band-to-band spectral peak (not shown in Fig. 5) tends to grow at a slightly higher rate.

Proportionality between light intensity and current can be expected when the emission quantum yield is independent of current, for example, if the internal quantum efficiency is close to unity. We can, therefore, conclude that the radiative transitions are closely associated with the tunneling current $I_2$. While this is true up to room temperature, it should be mentioned that above 300K the parameter $E_2$ approaches kT, hence the diffusion component may well be important at high temperature. As an example, the estimated value of $E_2$ at 340K is between kT and 2kT, well within the limits of thermal diffusion.

The pre-exponential factors $I_{s1}$ and $I_{s2}$ themselves

are temperature-dependent, as illustrated in Fig. 6 for the low-voltage current component in the old-generation LED #58. The prefactor current $I_{s1}$ varies from about $10^{-15}$ A at low temperatures to more than $10^{-11}$ A at 300K. Even more pronounced variation is obtained for $I_{s2}$, which changes from $10^{-25}$ A to $10^{-16}$ A over the same temperature range. Forward and reverse currents at a constant diode voltage of 2 V and –2 V are also temperature dependent. The dependence below 100K is very similar for both bias polarities, providing yet another evidence for the tunneling nature of the current.

Temperature sensitivity of I-V characteristics can be used practically as a way of measuring the temperature. The thermometric properties of the LEDs is demonstrated in Fig. 7, where the diode voltage is plotted vs temperature at a constant forward current of 1 μA. The average thermal sensitivity is around 5 mV/K. This value is about two times larger than typical thermal sensitivity of GaAs diodes.[12]

The reverse-bias part of the I-V characteristic at room temperature is shown in Fig. 8 for LED #58. No light emission was observed at reverse bias. The corresponding current density increases gradually from ~$10^{-8}$ A/cm$^2$ to 0.1 A/cm$^2$ in the voltage range up to 5 V. Such a large current variation with no apparent breakdown is not expected for the classical diffusion current or the generation-recombination current, but again may be attributed to a tunneling mechanism. This is confirmed by the solid curve in Fig. 8, which is drawn according to the theory for the dark current in photodiodes (see the Discussion section).

## Emission Spectra

The onset of visible yellow-green emission was observed by naked eye at low temperatures (T = 9–15K) for currents as low as 10–20 nA and voltage close to 2.4 V. At room temperature, the emission was observed at curents exceeding ~6 μA and voltage of 2.15 V. Evolution of the EL spectrum at ~15K is shown in Fig. 9. The position of EL peak for current ranging from 50 nA up to 10 μA changes from 2.43 to 2.71 eV. One can see the "blue" shift of sharp short-wavelength edge of the emission band indicating the filling of higher energy states as the diode voltage increases. At room temperature, the emission peak was observed to shift from 2.35 eV at 20 μA to 2.73 eV at 7.3 mA. It is worthwhile to note that for low bias range and at room temperature, the emission peak energy follows closely the value of applied bias V multiplied by the electron charge e. With further voltage increase, a separate short-wavelength peak appeared at ~3.2 eV. The latter is obviously associated with interband transitions in the InGaN active region and is much weaker in the new generation LEDs (see Fig. 10). The spectral bandwidth of the blue-band emission is 375 meV at 13K (10 μA) and

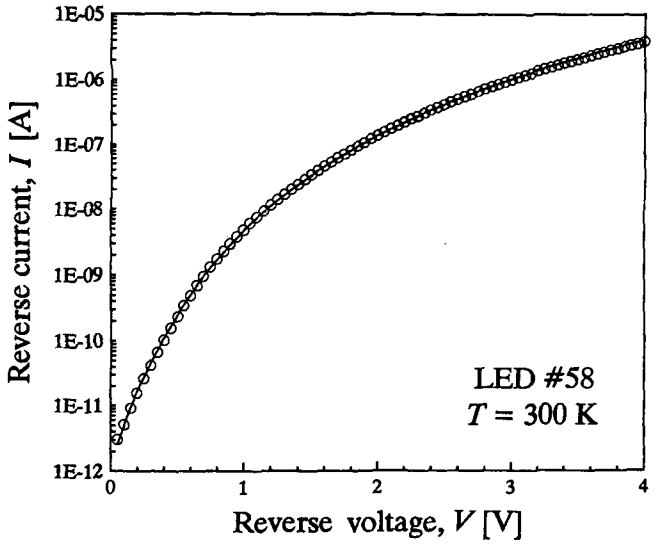


Fig. 8. Reverse branch of the I-V characteristic at room temperature for the old-generation LED #58. Open circles represent experimental points, while the solid curve is calculated using Eq. (8) with the following fitting parameters: a = 0.015 A, b = 15 V$^{1/2}$, $V_b$ = 7.7 V.

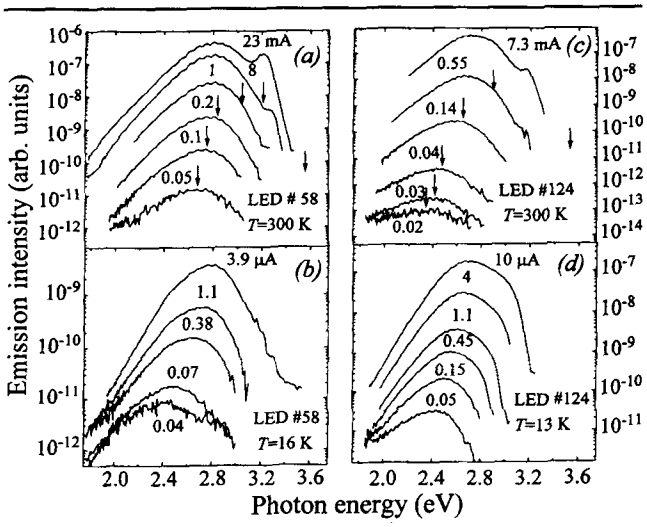


Fig. 9. Spectra of electroluminescence from LED at 16 (a) and 300K (b). Arrows indicate the eV position where V is the diode voltage value.

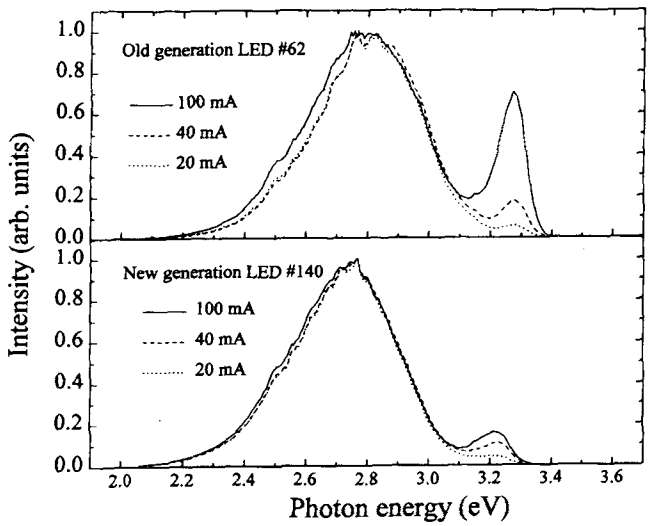


Fig. 10. Comparison between EL spectra from the old and new generations of Nichia NLPB-500 LEDs.

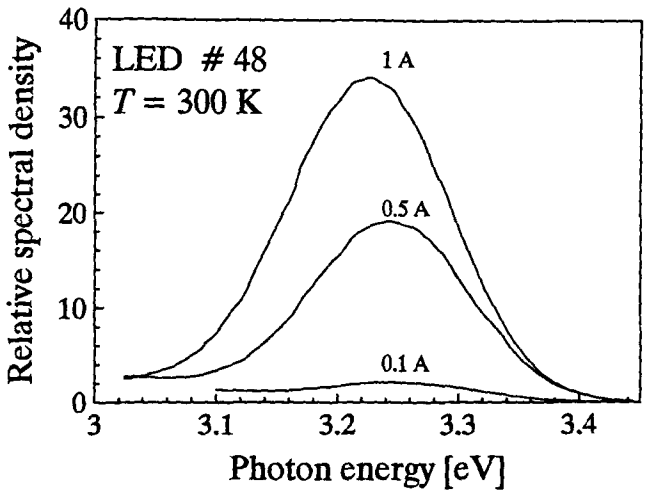


Fig. 11. Electroluminescence spectra of Nichia LED measured under pulsed current conditions (100 ns rectangular pulses, duty cycle $10^{-4}$).

between 300 and 340 meV at 300K, demonstrating a broadening of nonthermal nature. At low temperatures, the intensity of blue emission is almost an exponential function of the diode voltage V. The slope energy parameter, analogous to $E_2$ in Eq. (1b), is 129 meV for the LED #58 and ~140 meV for the LED #124, both at 13K. At room temperature, the low-voltage (L-V) curves differ from the exponential form, with the slope energy parameter increasing along with the diode voltage from (1–1.5)kT at low voltages to (2–3)kT at higher voltage. However, the slope of the main part of the dependence becomes close to $E_2$ when the correction for the series resistance is made, i.e., when the light intensity is plotted vs the junction voltage $V_j$ (cf. Fig. 5). The low-intensity (L–I) curves can be represented in the form of $I^m$ power functions with m = 1.55 at low temperatures (13–15K) and current-dependent m at 300K (m ≈ 3.5 at low intensities and m = 1–1.55 at higher intensities). When m is close to unity, it can be interpreted as a regime of a constant internal quantum efficiency. It should be stressed that m is indeed close to 1 when the light output intensity is plotted as a function of the medium-voltage current component $I_2$ rather than the total current I. This provides the main argument for our interpretation of $I_2$ as the current component responsible for light emission.

At very high current excitation (0.5–1.5 A) under pulsed conditions, the impurity-related band grows sublinearly with a more rapid growth of the 3.2-eV peaks.[13] The spectral shape of this short-wavelength band is shown in Fig. 11. It is close to a Gaussian with FWHM of ~160 meV at room temperature.

## DISCUSSION

### Low-Temperature Current Transport in Bulk Layers

The absence of a total freeze-out of carriers at temperatures as low as 9K would have been easy to understand if semiconducting materials used in the diode were degenerate. Carrier degeneracy is feasible in highly doped n-type side of the junction with shallow donor concentration exceeding $10^{19}$ $cm^{-3}$, but it is rather doubtful on the Mg-doped p-side, with relatively deep acceptor levels 150–180 meV above the valence band. This surprising observation is, however, consistent with recent data on bulk n-GaN[14] and p-InGaNs[15] conduction. In both cases, with the temperature decreasing from 300K down to about 100K, carrier concentration initially decreased and then quickly saturated at a level usually only two orders of magnitude lower than that at room temperature. It was concluded in Ref. 14 that a significant fraction of electron transport takes place by hopping in compensation centers leading to low mobility, compared to free carriers. This process becomes dominant at lower temperatures. We believe that a similar mechanism is responsible for the low temperature conductivity in p-type AlGaN and GaN. In addition, Tanaka et al.[16] observed nonlinearity of resistance in p-AlGaN at low temperatures, which can be of the same nature as the effect observed in the present work. The hopping mechanism of the carrier transport can be quite sensitive to applied electric field, hence low-temperature carrier mobility in passive regions may depend on the diode voltage even at low magnitude of the electrical field strength. Another contribution to resistance nonlinearity may arise from the photoconductivity effect in passive regions illuminated by the active region radiation. Recently, a noticeable photoresponse to a wide spectrum of incident light (from UV to near IR, including the entire visible spectrum) was reported for GaN epitaxial layers of both conductivity types.[17] Therefore, the visible spontaneous radiation propagating from the active region into the passive GaN layers can produce a change in their resistivity. Similar effect can be expected also in the AlGaN layers, but its magnitude is not known and is probably smaller than in GaN due to a larger bandgap energy of the alloy and smaller thickness of AlGaN layers. Finally, a current-dependent contribution to nonlinear resistance may be caused by Joule heating of the device.

### Tunneling Current Through p-n Junction

The temperature-independent slope of I-V curves in the semilogarithmic scale suggests the involvement of tunneling transport through the junction, and associated deep-level radiation emission is an evidence of tunneling to the deep levels. Such a mechanism of "excess current" was considered by Morgan[18] in heavily doped junctions where the shifting-peak emission is usually observed. The process may occur in the space-charge region of the junction through one or several intermediate (deep center) states. On the base of the tunneling probability calculation, the forward-bias excess current via deep levels was obtained in the following form:[18]

$$I \sim \exp\left\{-\frac{4\gamma}{3}\left[e\left(\frac{V_b - V}{E_\mu}\right)\right]^{3/2}\right\}, \qquad (2)$$

where $\gamma$ is a parameter dependent on carrier effective masses and approximately equal to 0.5, $V_b$ is the built-in potential barrier height, and $E_\mu$ is a bias-dependent characteristic energy of tunneling, associated with the electric field in the junction. In a simplified case of an asymmetric step junction, the current (2) may be expressed in the same manner as (1), namely,

$$I = I_1\left[\exp\left(eV_j / E_T\right) - 1\right], \qquad V_j \geq 0 \quad (3)$$

where $E_T$ is a characteristic energy constant, given by

$$E_T \approx 8e\hbar\sqrt{\frac{N_I}{m_T \varepsilon_r \varepsilon_0}}. \quad (4)$$

Here, $N_I$ is the ionized impurity concentration, $\varepsilon_r$, the static dielectric constant, and $\varepsilon_0$, the vacuum permittivity. The tunneling effective mass $m_T$ is the reduced effective mass of light holes and electrons for an interband (diagonal) tunneling or effective mass of carriers of one type for band-deep level tunneling. The expressions (3) and (4) are similar to those given in Refs. 19–21 for diagonal tunneling through an abrupt junction. Assuming $\varepsilon_r \approx 10$, $N_I = 10^{18}$ cm$^{-3}$, and $m_T = 0.27\ m_0$, we obtain $E_T = 185$ meV, very close to the experimental value of $E_1 = 180$ meV. Thus, it seems reasonable to explain the low-voltage current component by electrons tunneling to deep defect levels on the p-side of the junction without contributing to light emission. In order to tentatively interpret the medium-voltage current component (with parameter $E_2$ between 50 and 95 meV) that dominates at larger voltages (V > 2.9 V), we take $m_T$ equal to the hole effective mass $0.8m_0$. This gives an estimate of $E_T \approx 100$ meV, comparable to the values of $E_2$ in Table I (note that the estimate of $E_2$ is significantly less accurate than that of $E_1$ because of uncertainties associated with determination of the series resistance). Therefore, the medium-voltage component may be explained as a hole tunneling into n-InGaN, followed by the radiative transition via Zn-related levels.

Besides the "diagonal tunneling" mechanism in which both electrons and holes tunnel to the junction region and then recombine radiatively, another possible mechanism of carrier transport through the p-n junction is "multistep tunneling." This mechanism was originally proposed by Riben and Feucht[22] to describe tunneling current in forward biased Ge-GaAs heterojunctions. The model assumes a staircase path that consists of series of tunneling-recombination transitions, taking place between trapping levels and coupled to a series of vertical steps in which the electron loses energy by transferring from one level to the other. Such a process may occur if the trapping level density is sufficiently high. The multistep tunneling model was applied quite successfully for a number of diode structures,[23,24] although typically only for a low bias of a few hundreds mV.

As mentioned earlier, the low voltage component of the tunneling current in Nichia NLPB-500 LEDs can be described by Eq. (1a). Temperature dependence of the tunneling current $I_s$ can be very well approximated by the following exponential function:

$$I_s = I_0 e^{\frac{T}{T_0}}, \quad (5)$$

where $T_0 = 41.5$K and $I_0 = 3.6 \times 10^{-15}$ A.

In the multistep tunneling model, the tunneling current is described by the following expression:

$$I = AN_t e^{-C\sqrt{QV_b}} e^{C\sqrt{QV}} \quad (6)$$

$$C = \frac{8}{3\pi}\sqrt{\frac{m^*\varepsilon\varepsilon_0}{N_d}} \quad (7)$$

with $V_b$, the built-in voltage, $N_t$, the trap concentration, $N_d$, the donor concentration, and 1/Q, the number of steps required to cross the junction. Assuming the donor concentration of $10^{19}$ cm$^{-3}$, the fit of Eq. (6) to experimental results gives the value of 1/Q = 1.24, which means that one step would be sufficient to tunnel across the junction. The temperature dependence in the multistep tunneling model results from the temperature dependence of the built-in voltage. This in turn should be very close to the temperature dependence of the energy gap for GaN ($-4.5 \times 10^{-4}$ eV/K),[25] which gives $T_0$ in Eq. (5) equal to 404K, i.e., 10 times greater than the experimental value. We, therefore, conclude that the multistep tunneling model does not apply to the case of InGaN/AlGaN/GaN diodes.

As illustrated in Fig. 6, the reverse-bias current also has a tunneling nature. Other mechanisms, such as the generation-recombination and diffusion currents, are not observed as they are small in magnitude (due to a wide bandgap of constituent semiconductors) and have a rather weak voltage dependence. The interpretation of the reverse I-V characteristics at room temperature is given in Fig. 8, with the solid curve drawn according to the reverse-current tunneling model[26] for direct-gap semiconductors. The expression we used is

$$I_{rev}(V) = a\left(V + V_b\right)^{3/2} \exp\left[b/\left(V + V_b\right)^{1/2}\right], \quad (8)$$

where a and b are fitting parameters. It is remarkable that the entire curve can be very well approximated by a single set of parameters, including the built-in voltage $V_b = 0.77$ eV. Rigorously speaking, the approximation is valid only for $V > V_b$, whereas the fitting is excellent even at very low voltages. The value of $V_b$ may be associated with the barrier for tunneling of electrons into impurity level on the p-side with subsequent nonradiative recombination with holes.

## Optical Properties

A characteristic feature of the emission spectra is the dependence of the peak energy on the applied

bias. For the voltages lower than 2.6 eV at room temperature, the peak of the emission follows the value of applied voltage multiplied by the electron charge. For higher voltages, we observe even larger blue shift of the emission, and then at V ≈ 3 V the position of the EL peak stabilizes at ~2.8 eV. This kind of "shifting-peak" behavior[18-21] was attributed previously to "photon-assisted tunneling" of carriers across the junction. In the case of NLPB-500 LEDs, visible emission is provided by recombination through Zn-related levels, therefore the hole tunneling to these levels from the p-side should occur. These tunnelinug transitions are followed by radiative capture of electrons from the conduction band and (at low temperature) from donor impurity band to the Zn-related levels. A large bandwidth of the EL is related to large lattice coupling of the Zn state to the lattice[11] both in GaN and in InGaN.[6] Some contribution into the spectral bandwidth can be related to the composition fluctuations occurring in the InGaN alloy.

Several Zn-related levels can contribute to the emission band. Our earlier work[6] indicates that probably three of them are involved in the blue and green emission. Contribution from each level is composed of a zero-phonon line and a number of phonon replicas. As a result, each level produces a broad-envelope contour including a series of broadened individual lines. The distance between individual spectral components corresponds to the phonon energy. The energy of localized phonons $E_\omega$ at the two lower Zn-related levels is between 75 and 90 meV in GaN,[11] and approximately fall in the same range for $In_{0.06}Ga_{0.94}N$,[6] as determined by the analysis of photoluminescence spectra. The envelope peak is shifted from the zero-phonon line toward the "red" by $\sim\Lambda E_\omega$, where $\Lambda$ is the electron-phonon coupling coefficient for the particular level. The envelope bandwidth may be estimated for any of two levels by a quantity $\sim 1.5\Lambda E_\omega$, which gives about 0.3 eV for $\Lambda = 2.7$ and $E_\omega = 75$ meV.[6] As the energy distance $\Delta E$ between two lower levels is ~0.3 eV, the total spectral width of the two overlapping bands will be about $2\Lambda E_\omega + \Delta E = 0.6$ eV. When the broadening of an individual spectral component is comparable with the distance between them, the series structure of the total band cannot be clear, and the overall width is approximately the same as the above quantity of 0.6 eV. It is indeed the case at room temperature, as the observed blue emission line has a spectral width about 0.6 eV.

Relative contributions of two or three series may change with temperature, hence the peak of the total emission spectrum can move in a way different than the temperature variation of the bandgap. Possibly due to this the blue-emission peak shift between 10 and 300K is only 30 meV whereas a change in the bandgap is ~80 meV. The broadening of the individual spectral component is about 50–75 meV. This can be a result of both alloy mixing effect and of an increased strain due to a lattice misfit.

The short-wavelength spectral band appearing in the EL spectrum at high currents is most likely related to the band-to-band emission from the InGaN active layer. The peak photon energy corresponds to 3.2 eV which is close to the bandgap energy of the alloy. The spectral bandwidth of the edge emission is, however, much larger than it is expected from the band-to-band radiation model with a primarily thermal broadening. In the latter case the calculated bandwidth is ~2.1 kT, which is twice smaller than the observed value. The band shape is close to a Gaussian, and the energy parameter of the Gaussian is about 68 meV. An inhomogeneous contribution into the line broadening can be tentatively attributed to the composition fluctuations.

Concluding this part, we observe significant differences in both electrical and optical properties between the old and new generation devices. New generation is characterized by a higher series resistance, and a lower UV component of emission. The increase of a resistance in new generation devices can be related to the improvement of their quality and decrease of the threading defects density which can provide a parallel path for the current flowing across the highly resistive p-type layers. The weakening of the UV component of emitted light in new generation devices is associated with the increased zinc doping of the active layer.[27]

## CONCLUSIONS

In conclusion, we studied the electrical and optical characteristics of InGaN/AlGaN/GaN double-heterostructure LEDs in a wide current density and temperature ranges (with no complete freeze-out even at the lowest temperatures). Tunneling is identified as a dominant mechanism of carrier transport through the junction at both forward and reverse bias. In both cases, the involvement of states in the forbidden band is identified. In the forward-bias current, we can identify at least two exponential components. The low-voltage current component seems to be associated with electrons tunneling to nonradiative defect states at the p-side. The medium-voltage current component, appearing above 10 mA at room temperature, seems to be related to blue light emission via Zn-related centers. A shifting spectral peak of optical emission is consistent with the tunneling nature of electrical characteristics.

## ACKNOWLEDGMENTS

We would like to thank Professor Kevin Malloy for his collaboration on this project. Support of the Advanced Research Projects Agency (ARPA) under the Optoelectronic Materials Center program and of the New Energy and Industrial Technology Organization (NEDO) of Japan is gratefully acknowledged.

## REFERENCES

1. S. Nakamura, T. Mukai and M. Senoh, *Jpn. J. Appl. Phys.* 30, L1998 (1991); S. Nakamura, M. Senoh and T. Mukai, *Appl. Phys. Lett.* 62, 2390 (1993); S. Nakamura, T. Mukai and M. Senoh, *J. Appl. Phys.* 76, 8189 (1994).
2. S. Nakamura, T. Mukai and M. Senoh, *Appl. Phys. Lett.* 64, 1687 (1994); S. Nakamura, *J. Cryst. Growth* 145, 911 (1994).

3. S. Nakamura, M. Senoh, S. Nagahama, N. Iwasa, T. Yamada, T. Matsushita, H. Kiyoku and Y. Sugimoto, *Jpn. J. Appl. Phys.* Pt. 2 (Lett.) 35, L74 (1996); S. Nakamura, M. Senoh, S. Nagahama, N. Iwasa, and T. Yamada, *Appl. Phys. Lett.* 68, 3269 (1996); S. Nakamura, *J. Vac. Sci. Technol. A* 13, 705 (1995).
4. P. Shah, V. Mitin, M. Grupen, G.H. Song and K. Hess, *J. Appl. Phys.* 79, 2755 (1996).
5. L. Lee, M. Osiński and K. J. Malloy, *Conf. Proc., LEOS'94 7th Annual Mtg.,* Boston, MA, 31 Oct.–3 Nov., 1994, Vol. 1, (1994), p. 332.
6. P.G. Eliseev, V.A. Smagley. P. Perlin, P. Sartori and M. Osiński *Physics and Simulation of Optoelectronic Devices IV,* eds. W.W. Chow and M. Osiński San Jose, CA, 29 Jan.–2 Feb., 1996, 2693, (SPIE, 1996), p. 97.
7. H.C. Casey, Jr., J. Muth, S. Krishnankutty and J.M. Zavada, *Appl. Phys. Lett* 68, 2867 (1996).
8. P. Perlin, M. Osiński, P. G. Eliseev, *Sr.* A. Smagley, J. Mu, M. Banas, and P. Sartori, *Appl. Phys. Lett* 69, 1680 (1996).
9. M. Osiński and P.G. Eliseev, *Abstracts, Topical Workshop on III-V Nitrides TWN'95,* Nagoya, Japan, 21–23 Sept., 1995, p. C-5.1.
10. J.I. Pankove, J.E. Birkeyheiser and E.A. Miller, *J. Appl. Phys.* 45, 1280 (1974).
11. B. Monemar, O. Lagerstedt and H.P. Gislason, *J. Appl. Phys.* 51, 625 (1980).
12. B.G. Cohen, W.B. Snow and A.R. Tretola, *Rev. Sci. Instr.* 34, 1091 (1963).
13. D.L. Barton, J. Zeller, B.S. Phillips, P.-C. Chiu, S. Askar, D.-S. Lee, M. Osiński and K.J. Malloy, *Proc. 33rd Annual IEEE Intl. Reliability Physics Symp.,* Las Vegas, NV, 4–6 April 1995, p. 191.
14. J. Moluar, T. Lei and T.D. Moustakas, *Appl. Phys. Lett.* 62, 72 (1993).
15. S. Yamasaki, S. Asamu, N. Shibata, M. Koike, K. Manabe, T. Tanaka, H. Amano and I. Akasaki, *Appl. Phys. Lett.* 66, 1112 (1995).
16. T. Tanaka, A. Watanabe, H. Amano, Y. Kobayashi, I. Akasaki, S. Yamazaki and M. Koike, *Appl. Phys. Lett.* 65, 593 (1994).
17. C.H. Qiu, C. Hoggatt, W. Melton, M.W. Leksono and J.I. Pankove, *Appl. Phys. Lett.* 66, 2712 (1995).
18. T.N. Morgan, *Phys. Rev.* 148, 890 (1966).
19. R.C.C. Leite, J.C. Sarace, D.H. Olson, B.G. Cohen, J.M. Whelan and A. Yariv, *Phys. Rev.* 137, 1583 (1965).
20. D.J. Dumin and G.L. Pearson, *J. Appl. Phys.* 36, 3418 (1965).
21. H.C. Casey, Jr. and D.J. Silversmith, *J. Appl. Phys.* 40, 241 (1969).
22. A.R. Riben and D.L. Feucht, *Int. J. Electron.* 20, 583, (1966).
23. A.R. Riben and D.L. Feucht, *Solid. State Electron.* 9, 1055, (1966).
24. G. Sarusi, A. Zemel, A. Sher and D. Eger, *J. Appl. Phys.* 76, 4420, 1994).
25. H. Teisseyre, P. Perlin, T. Suski, I. Grzegory, S. Porowski, J. Jun, A. Pietraszko and T.D. Moustakas, *J. Appl. Phys* 76, 2429 (1994).
26. S.R. Forrest, M. DiDomenico, Jr, R.G. Smith and H.J. Stocker, *Appl. Phys. Lett.* 36, 580 (1980).
27. S. Nakamura, private communication.